Role of Tensile Stress in DNA Nanoresonators for Epigenetic Studies

*Francesca Legittimo[a], Monica Marini[b], Stefano Stassi[a], Mauro Tortello[a], John E. Sader[c], Paul Ashby[d], Behzad Rad[d], Corie Y. Ralston[d], Enzo Di Fabrizio[a], Carlo Ricciardi[a,]**

[a]*Politecnico di Torino, Department of Applied Science and Technologies (DISAT), Corso Duca degli Abruzzi 24, 10129 Torino (Italy)*

[b] *Advanced Materials Metrology and Life Sciences Division, Istituto Nazionale di Ricerca Metrologica (INRiM), Strada delle Cacce 91, 10135 Torino, Italy*

[c] *Graduate Aerospace Laboratories and Department of Applied Physics, California Institute of Technology, Pasadena, CA 91125, USA*

[d] *Molecular Foundry, Lawrence Berkeley National Laboratory, 67 Cyclotron Road, Berkeley, California, 94720, USA*

KEYWORDS: Epigenetics, DNA methylation, DNA nanoresonators, nanomechanical sensing, AFM force curve.

Abstract

The evaluation of epigenetic features such as DNA methylation is becoming increasingly important in many biochemical processes like gene expression and transcription, as well as in several diseases like schizophrenia or diabetes. Here we report that self-assembled nanomechanical resonators entirely composed of DNA molecules can be used to explore gross change in DNA methylation levels (0-25-50%), while a careful control of tensile stress is needed to reduce the variability of resonance frequency for rigorous quantification. The effect of the tensile stress retained by the suspended DNA nanoresonators, on application of the technique, is extensively explored using a combination of laser Doppler vibrometry and atomic force spectroscopy. DNA nanoresonators are real time, label free sensors, and could avoid chemical functionalization and sample amplification. Therefore, they may represent a key enabling technology for future massive epigenetic studies needed for example to evaluate the consequences on human genome of a prolonged exposure to heavy metals in a contaminated industrial site.

Introduction

DNA epigenetic features are nowadays largely defined as modifications of the gene functions which are mitotically or meiotically heritable, but do not affect the DNA sequence[1]. Nevertheless, they are of fundamental importance in the diversification of gene expression of different cells and tissues in multicellular organisms[2]. Among the most well-known epigenetic features, DNA methylation consists of a covalent modification of the cytosine nucleotide at the 5' carbon position, where a hydrogen atom is substituted with a methyl group. In humans cells, 70%–80% of all CpG dinucleotides in the genome are affected by this modification[3], which can alter the structure and stability of chromatin, an essential step for transcription. Physiological levels of DNA methylation

are therefore essential to guarantee many biological functions[4] including genome stability, imprinting, and the overall correct mammalian development[5]. The role of methylation is particularly crucial in brain development since changes in methylation levels are associated with brain plasticity, as well as learning and memory processes[6,7]. Furthermore, it is well known that aberrant methylation levels are associated with several severe diseases. For example, hypermethylation of CpG islands in genes promoter regions is the most widespread epigenetic modification occurring in human neoplasms since it is linked to incorrect transcriptional suppression of genes[8]. Other conditions characterized by hypo or hyper-DNA methylation include but are not limited to schizophrenia[4] and immune diseases like multiple sclerosis[9] and type 1 diabetes, for which a substantial enrichment of DNA methylation has been found in monozygotic twins affected by the disease, contrarily to their unaffected twin siblings[10].

While the genetic information stored by the base-pairs stacking is fixed from birth, the DNA methylation level and more in general DNA epigenetic features can vary through a lifetime, due to interaction with the environment. This eventuality is reported for exposition to heavy metals[11] or pesticides[7], as well as for the development of Post-Traumatic Stress Disorder (PTSD) [12]. Furthermore, environmental-determined epigenetic modifications can be inherited by offspring, even if the driving stimuli occur before conception, as verified in Ref. 13. In that study, the authors exposed mice to odor fear conditioning prior to conception and the two following generations showed an enhanced behavioral sensitivity to the conditioned odor used to treat their ancestor. The outcome of the experiment was found to be dependent on CpG hypomethylation in the *Olfr151* gene of the first and second generation of mice sperm DNA.

In light of this evidence, it is clear that having an accessible tool for the investigation of DNA methylation levels would be of fundamental importance in early diagnosis of a large number of

diseases, for which this modification can be used as a biomarker. The techniques commonly used to evaluate genomic methylation levels, as pyrosequencing and methylation specific High Resolution Melting Analysis, rely on the definition of appropriate primers, quantitative PCR and bisulfite DNA conversion[14]. They can provide single base methylation resolution. However, a rapid, cheap, and sensitive tool for large studies of potentially clinically relevant methylation level alteration in genomic DNA is missing.

In the last few years, advancement in nanomaterials characterization and the exploitation of engineered Super Hydrophobic Substrates (SHS) has enabled the self-assembly of mechanical nanoresonators entirely composed of DNA molecules. The vibrometric analysis of these peculiar suspended nanostructures has been recently used to successfully investigate the structural effects of DNA-ligand interaction[15] and of temperature-dependent features such as melting temperature[16]. In this study, we show that the same approach could be efficiently used to explore gross change in DNA methylation levels (0-25-50%), when certain working conditions are fulfilled. In particular, the effect of the tensile tension retained by the suspended DNA nanoresonators on the applicability of the technique is extensively explored thanks to the combination of laser Doppler vibrometry and atomic force spectroscopy. Since DNA nanoresonators are real time, label free sensors, and could avoid chemical functionalization and sample amplification, they may represent a key enabling technology for future massive epigenetic studies. These are needed, for example, to evaluate the consequences on the human genome of prolonged exposure to heavy metals in a contaminated industrial site.

Experimental methods

Suspended DNA nanoresonators were produced starting from solutions of λDNA molecules (48502 bp sequence, New England Biolabs (NEB), Ipswich, MA, USA), at different levels of methylation: approximately 50%, 25% (dam- λDNA), 0% (dam- dcm- λDNA). The DNA precursor was diluted in buffer solution (PBS 1x, pH~7) at a final concentration of 50ng/μL and pre-heated for 10 minutes at 65°C to prevent any undesired hybridization between partially complementary sequences. After 30 minutes of incubation at 37°C, a 5 μL drop was deposited on the top of an SHS and allowed to evaporate in a controlled environment (21°C and ~50% RH). The SHS, produced as previously reported[17,18], is composed of silicon micropillars (diameter of 6 μm), uniformly distributed over the wafer in concentric circles. The edge-to-edge interpillar distance in the radial direction is designed to be 12μm. This geometrical pattern forces the drop to reduce its volume by means of discrete jumps from one concentric circle of pillars to a closer internal circle[17,19]. During these events, the DNA molecules in solution are dragged between one external pillar and a proximal one[20], resulting in self-assembly of suspended bundles made of multiple DNA molecules (see Fig.1 and S1). The preferential orientation of the bundles is favored by the direction of evaporation of the drop, but it is made possible by the interpillar distance which is designed to be lower than the DNA length, in this case approximately equal to 16μm. The self-assembled suspended DNA bundles, with no metal coating, are imaged by Scanning Electron Microscopy (Fesem Supra 40, Zeiss, Oberkochen, Germany) with acceleration voltage of 5keV, working distance equal to 2.5mm, and aperture size of 30μm. The dimensions (diameter and length) of each bundle are measured from the SEM images by means of ImageJ and Gatan Microscopy Suite Software, free version from Amatek.

A laser Doppler vibrometer (MSA-500, Polytec Gmbh, Waldbronn, Germany, nominal displacement and velocity resolutions of <0.4pm/$\sqrt{Hz}$ and <1μm/s, respectively) was used to

perform the vibrometrical analysis of the DNA resonators in air. The laser is focused on the surface of the bundles through a 100× objective lens (PLAN Apochromat, 0.55 N.A., 13mm WD, Motic., Hong Kong); its laser spot size on the DNA resonators is approximately 1μm in diameter, such that highest reflectivity of the laser beam is roughly the 60%. No actuation is performed for the measurements; the thermomechanical vibration spectrum is obtained using 500 averages, to maximize the signal-to-noise ratio. The bandwidth is fixed at 10MHz with 204800 FFT lines and a spectral resolution of approximately 48Hz.

The force curve analysis was performed using an Asylum Cypher ES Atomic Force Microscope (AFM - Oxford Instrument). The tip used to perform the measurement was a Tap150Al-G (Budget Sensor), a micromachined monolithic silicon AFM probe for soft tapping mode operation; the nominal radius and spring constant were respectively 5nm and 5N/m. The bundles were firstly imaged in tapping mode and then a force-curve map was performed in contact mode with a starting distance of 2 μm, scan speed 1Hz and trigger force equal to 10nN. The lines of the map (usually 6) probe the entire length of the image, from one pillar to the other by means of typically 32 points. The aspect ratio of the net is further increased to 64×1, in order to be sure to probe the central part of the beam through the central line. The contribution of cantilever bending during the force-curve analysis was automatically removed by the instrument software. Further information about the methodology of the AFM force-curve analysis can be found in the Supporting Information (Fig. S3-S7).

Results and discussion

Vibrational properties of DNA nanoresonators

DNA nanoresonators were obtained by means of a well-established self-assembly technique described in details elsewhere[17,21,22]. The process requires deposition of a solution droplet,

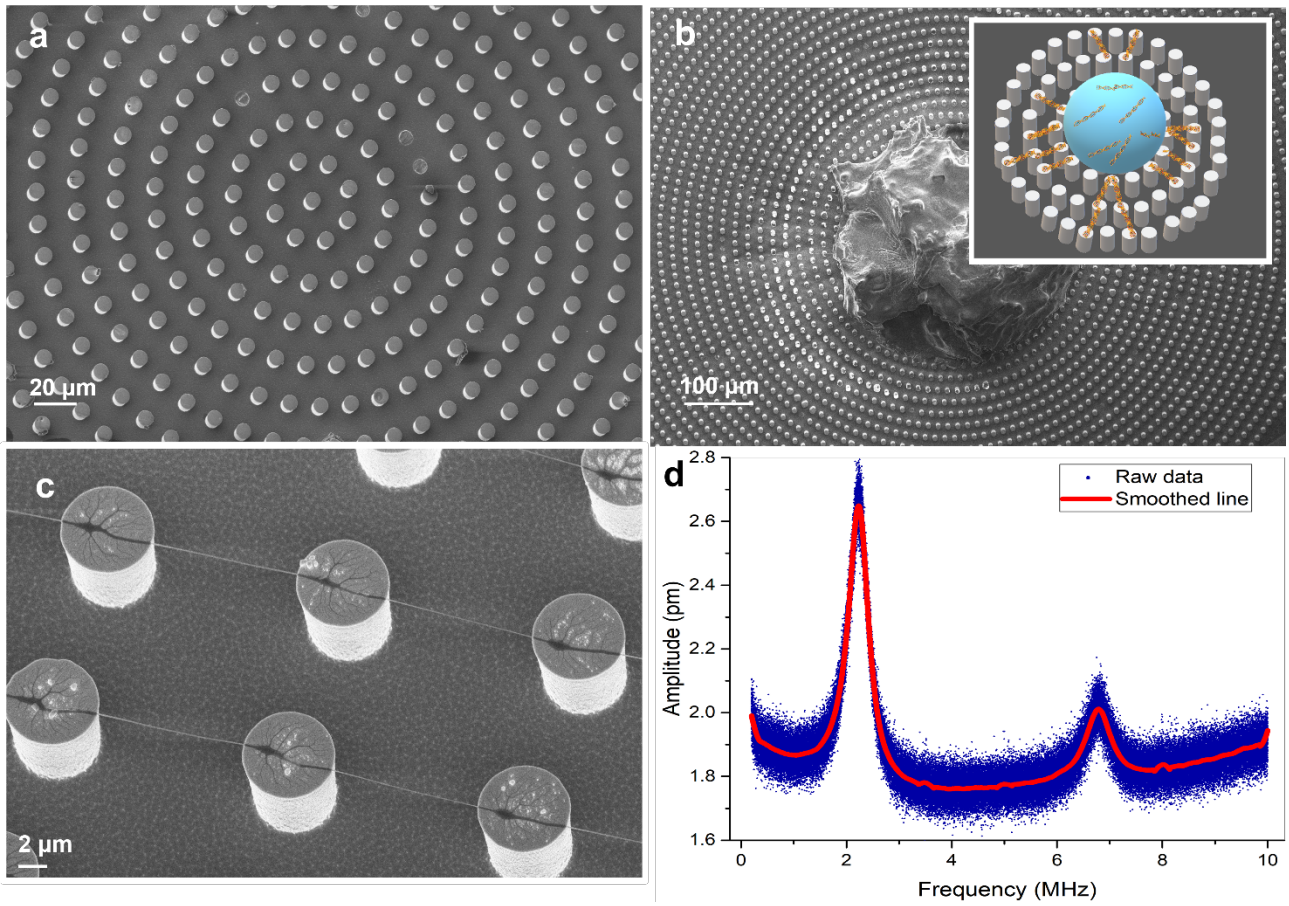

Figure 1. a) SEM image of the central part of an SHS showing the geometrical distribution of the silicon micropillars. b) Outcome of the suspension process: the central residue contains the non-suspended materials surrounded by the suspended bundles; in the inset, a cartoon of the suspension. c) Tilted SEM image of 4 bundles with their supporting pillars: on their surface it is possible to see that the suspended bundles are composed of several sub-fibers attached to the pillars at different points and then merged in a main suspended body. d) Typical vibrational spectrum of a DNA nanoresonator acquired in air environment. The blue points are the raw data, while the red line represents the smoothed spectrum; a baseline is subtracted before performing the Lorentzian fit of the square amplitude of the signal.

containing the desired DNA molecules, on the surface of a SHS, composed by concentric circles of silicon micropillars, Teflon coated to increase their hydrophobicity (Fig. 1a).

At the end of the drying process, the non-suspended materials precipitated in the middle of the SHS, forming a visible residue surrounded by all the radially distributed DNA bundles. The bundles have lengths approximately equal to the inter-pillar distance (12 μm) and diameters ranging from 20 nm to 180 nm (Fig. 1b). A cartoon of the suspension process is shown in the inset of Fig. 1b. As previously proved by means of HRTEM[21,23], the DNA molecules inside the bundles are distributed in concentric shells, divided by solvation layers. Fig. 1c reports a tilted SEM image of four bundles together with their supporting pillars, whose patterns on the surface provide evidence of the suspension mechanism. It is noteworthy that several DNA molecules first attached to the pillars in different locations, and then merged into the main bundle. This is due to the drop partial evaporation from one pillar circumference to the inner one (inset in Fig. 1b and Fig. S1). Furthermore, Fig. 1c clearly shows that the DNA suspended bundles can be viewed as double-clamped nanoresonators. A typical vibrational spectrum of such a nanostructure, obtained in air environment, is reported in Fig. 1d: despite the fact that the first and second mode resonance peaks, centered respectively in 2.10 and 5.46 MHz, have amplitudes as low as few picometers, they clearly emerge from the background thermal noise. The quality factors of these structures are in the range of 1 to 5 and the experimental uncertainty associated with the resonance frequency is in the order of 2%, as detailed in previous work[16].

In this work, the vibrational analysis was performed on 117 nanoresonators, with diameter ranging from 40 to 130 nm, composed of λDNA molecules with a methylation level equal to 50%, 25% and 0%. They were all produced starting from solutions containing the buffering agent PBS, pH ≈ 7, which mimics the cellular environment. The three sample sets contained respectively 44,

49 and 24 bundles; the latter one is less numerous since the totally unmethylated DNA molecules provide less stable bundles. Tables S1, S2, S3 report each bundle sizes (L, D) and first mode resonance frequency (f_1), while the average values of these parameters for each methylation level are reported in Table1.

Table 1. Average length L, diameter D and resonance frequency f_1 for the 3 classes of analyzed samples. The uncertainties correspond to the standard deviations.

Methylation	***L* (μm)**	***D* (nm)**	f_1 **(MHz)**
0%	11.86 ± 0.50	96 ± 16	1.83 ± 0.67
25%	11.80 ± 0.63	90 ± 20	2.67 ± 0.41
50%	11.31 ± 0.67	94 ± 20	3.11 ± 0.70

The dependence of the fundamental resonance frequency of all measured DNA nanoresonators (diameter D in the range $40<D<130$ nm) as a function of different methylation levels is reported in Fig. 2a: visibly, the average resonance frequency monotonically increases with the percentage of DNA methylation. The average and median values for the three sample sets are clearly identifiable, implying that the resonance frequency might be used as a reasonable figure of merit to distinguish substantial variations in the methylation level of DNA molecules suspended in PBS buffer solution, i.e. in physiological conditions.

Considering the DNA nanoresonators as stress-free double-clamped beams, their resonance frequency is

$$f_n = \frac{\lambda_n^2}{2\pi L^2}\sqrt{\frac{EI}{\rho A}} \quad (1)$$

where L, E, ρ, I and A are the length, the Young's modulus, the mass density, the second moment of area and the cross sectional area of the bundles, respectively, while λ_n is the modal factor satisfying, $\cos\lambda_n \cosh\lambda_n = 1$, for $n = 1, 2, 3, \ldots$. Under this very common approximation, the first mode resonance frequency can be used to estimate the resonator stiffness once the density and dimensions are known. Therefore, the monotonic increasing relationship between average resonance frequency and methylation level shown in Fig. 2a is consistent with theoretical and experimental findings previously reported in the literature[4,24]. These findings state that the steric action of the methyl group on the main groove of DNA increases the relative intrastrand stacking stability of the double helix, thus resulting in an enhanced stiffness of the entire structure.

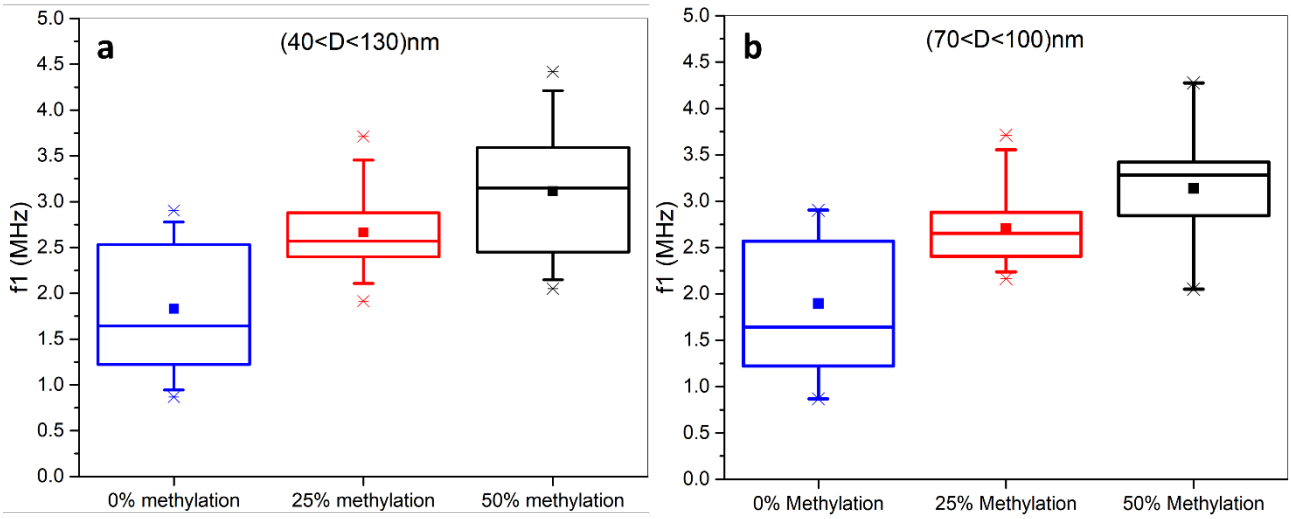

Figure 2. a) Resonance frequencies box plot of all the DNA nanoresonators (diameter D in the range 40<D<130 nm) as a function of the methylation level. The boxes represent the 25th-75th interquartile range, containing the average value and the median line, while the bars stand for the 5th and 95th percentiles, and the crosses show the maximum and minimum values. b) Resonance frequencies box plot as a function of methylation level of the DNA nanoresonators with a comparable diameter D (range 70<D<100 nm) to highlight the impact of bundles' geometrical variability.

Using the same approach, Stassi et al.[15] measured a Young's modulus on the order of 5GPa for the DNA bundles composed of molecules at 50% of methylation. However, it is clear that no rigorous quantification exists for the data shown in Fig. 2a since the interquartile ranges of 0, 25 and 50% methylated DNA bundles frequently overlap; due to the high intrinsic variability of the resonance frequency in each set of samples, which can span ranges of even 2MHz. Looking at eq. (1) and considering the typical irregularity of self-assembly processes, it is expected that the main contribution to frequency variability could rely on the distribution of bundle dimensions. In particular, while the variation in length can be neglected since it is limited by the fixed distance between the pillars, the intrinsic variability in bundles diameter is much larger (relative deviation of about 5% to 20%, respectively, from Table 1).

In order to explore the influence of the geometry, Fig. 2b limits the resonance frequencies box plot as a function of methylation level for DNA nanoresonators with a comparable diameter D in the range 70-100 nm (the most abundant class, as detailed in Fig. S2a,b,c).

The result is very similar to Fig. 2a: while the monotonic behavior of the average resonance frequency as a function of the methylation is confirmed, the interquartile ranges remain large for a quantitative analysis. The same conclusion holds for the less abundant class of diameters in the range 100-130 nm, reported for clarity in the Supporting Information (Fig. S2d).

Further evidence that the variability of the resonance frequencies cannot be ascribed uniquely to the different sizes of the bundles is given by DNA nanoresonators that show very different resonance frequencies, despite having comparable sizes. An example can be found in Fig. 3, which reports the spectra of two bundles corresponding to bundles 32 and 27 in Table S1, with the same 50% of methylation. They both have a diameter of approximately 100 nm (see the insets in Fig. 3a,b), but their resonance frequencies differ by approximately 2MHz. This is clearly shown in Fig.

3c, in which the vibration signals of the two resonators are normalized to the maximum amplitudes to simplify the comparison.

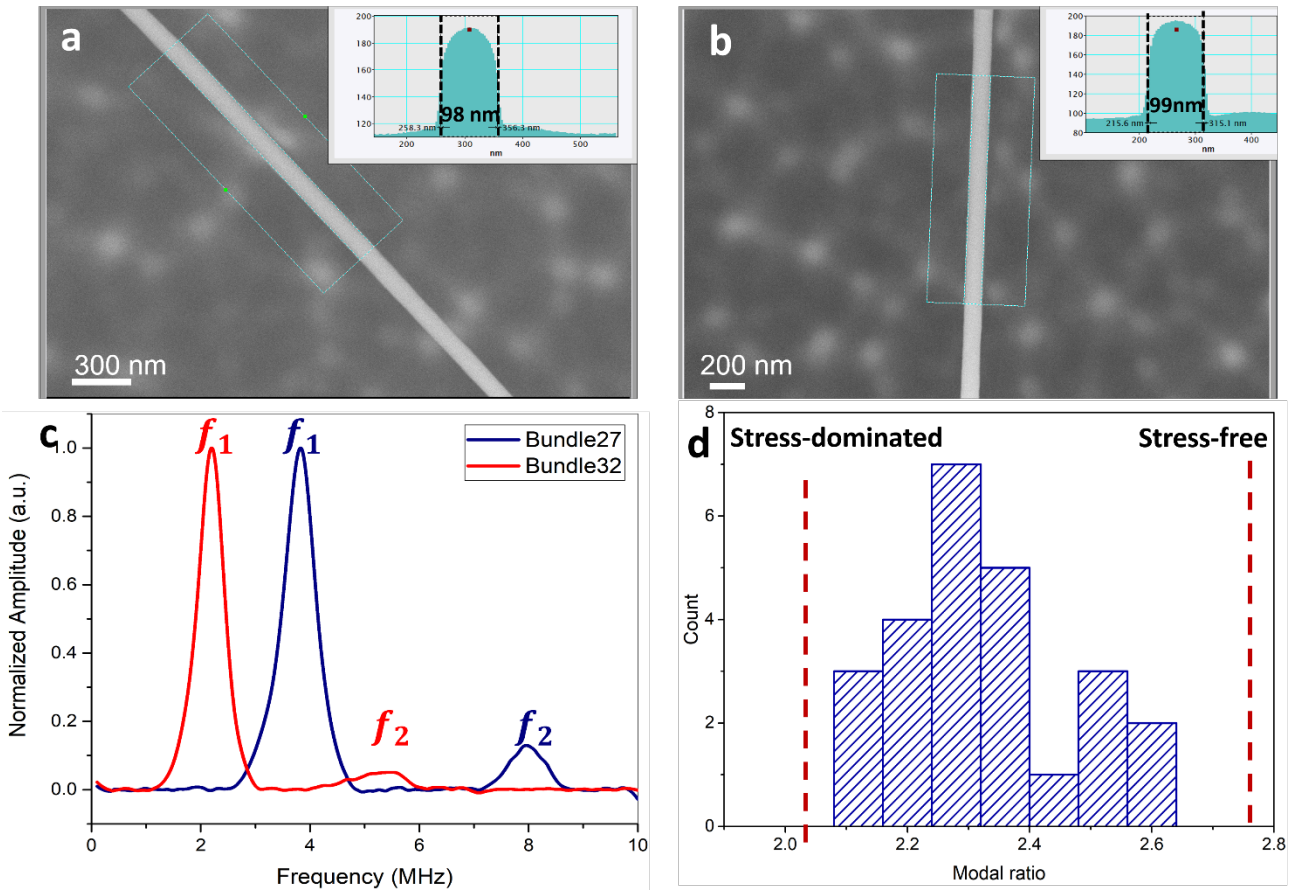

Figure 3. a) SEM image of DNA bundle 27 with 50% of methylation; the inset shows the evaluation of the diameter performed through the software Gatan Microscopy Suite (98nm). b) SEM image of DNA bundle 32 with 50% of methylation; the inset shows the evaluation of the diameter performed through the software Gatan Microscopy Suite (99.5nm). c) Normalized and smoothed vibrational spectra of bundle 27 and bundle 32: the first and second resonant modes are indicated as f_1 and f_2. d) Histogram of the modal ratio of the DNA bundles for which the second mode was recorded; the dotted lines correspond to the two extreme cases: $f_2/f_1 = 2$ (stress-dominated resonators) and $f_2/f_1 = 2.76$ (stress-free resonators).

An interesting point to analyze in DNA bundles is the modal ratio between the first (f_1) and the second (f_2) resonance modes, since it can give information related to the presence of stress in the resonator. Such stress would affect the resonance frequency with respect to the values predicted from eq. (1). Looking at the vibration spectra, the modal ratio of bundle 32 was 2.14, i.e. very close to 2 which is the theoretical modal ratio of a doubly-clamped beam dominated by the stress, i.e. in the so-called *string* configuration. On the other hand, for bundle 27, the value of this figure of merit is equal to 2.45, i.e. closer to 2.76, the value expected for perfectly double-clamped beam which can be considered *stress-free*. The analysis of the modal ratio was conducted for all the bundles for which also the second resonant mode was measurable: the results are graphically shown in the histogram of Fig. 3d and are reported in the last columns of Tables S1, S2, and S3. As a matter of fact, the modal ratio f_2/f_1 spans from 2.1 to 2.6, strongly suggesting that the DNA bundles retain a variable amount of intrinsic tensile stress σ. Such a configuration is analytically described by the following equation[25]:

$$f_n = \frac{\lambda_n^2}{2\pi}\sqrt{\frac{EI}{\rho A}}\sqrt{1+\frac{\sigma A L^2}{EI\lambda_n^2}} \quad . \qquad (2)$$

According to this equation, bundles with a higher retained/residual stress σ would show a higher resonance frequency. This is consistent with bundle 32 which, with a modal ratio of 2.14, has first a mode resonance frequency almost double that of bundle 27, which showed a larger f_2/f_1. For a bundle with typical dimensions of D ≈ 90 nm and L ≈ 11.7 mm, and Young's modulus fixed to 4.9 GPa (value found by Stassi et al.[15]), a tensile stress roughly between 1 and 6 MPa would justify the experimental modal ratio variation in the range 2.1-2.6. Further information about the analytical relation between stress and modal ratio is reported in Fig. S3. To further elucidate the mechanical properties of DNA bundles, an independent analysis for measuring E and σ is needed.

AFM force curve analysis of suspended DNA bundles

In order to estimate the retained/residual stress in the DNA nanoresonators, AFM force-displacement (F-δ) curves were performed on a new set of suspended DNA bundles at 50% methylation. This technique has been widely exploited in the last few years to study the mechanical elastic behavior of a variety of double-clamped nanowires (NWs) systems, by measuring their bending response under the load of an AFM cantilever tip[26–29]. According to elastic-beam theory, a point load F applied in the midpoint of a double-clamped beam induces a bending of the beam δ such that $F = 192\frac{EI}{L^3}\delta$.[30] However, this simple model does not take into account the tensile force that is induced by the stretching of the beam during its displacement and that can affect the beam mechanical response, eventually leading to non-linearity of the F-δ curves[31,32]. A first solution to this problem was developed by Heidelberg et al. [33], while the model was updated by Mills et al. [34] in order to consider the presence of possible intrinsic tensile or compressive stress retained by the NWs. As reported in Ref. 34, the force F applied in the center of the suspended beam is linked to its deflection δ according to:

$$F = 192\frac{EI}{L^3}f(\alpha)\delta_{center} \tag{3}$$

with

$$f(\alpha) = \frac{\alpha}{48 - \frac{192\tanh\left(\frac{\sqrt{\alpha}}{4}\right)}{\sqrt{\alpha}}} \tag{4}$$

where α is a parameter composed of two terms:

$$\alpha = \alpha_m + \alpha_0 = \frac{6\left(\frac{2\delta}{R}\right)^2\left(140+\frac{2\delta}{R}\right)}{350+3\left(\frac{2\delta}{R}\right)} + \frac{TL^2}{EI}. \tag{5}$$

The first term (α_m) accounts for the stress induced by the measurement as a result of a finite displacement that starts to play an significant role when δ is comparable to the beam radius R. The second term (α_0) is related to the intrinsic tension (T) held by the NW and is independent of the AFM analysis. It follows that it is possible to perform a parametric fit of the contact part of the *F*-

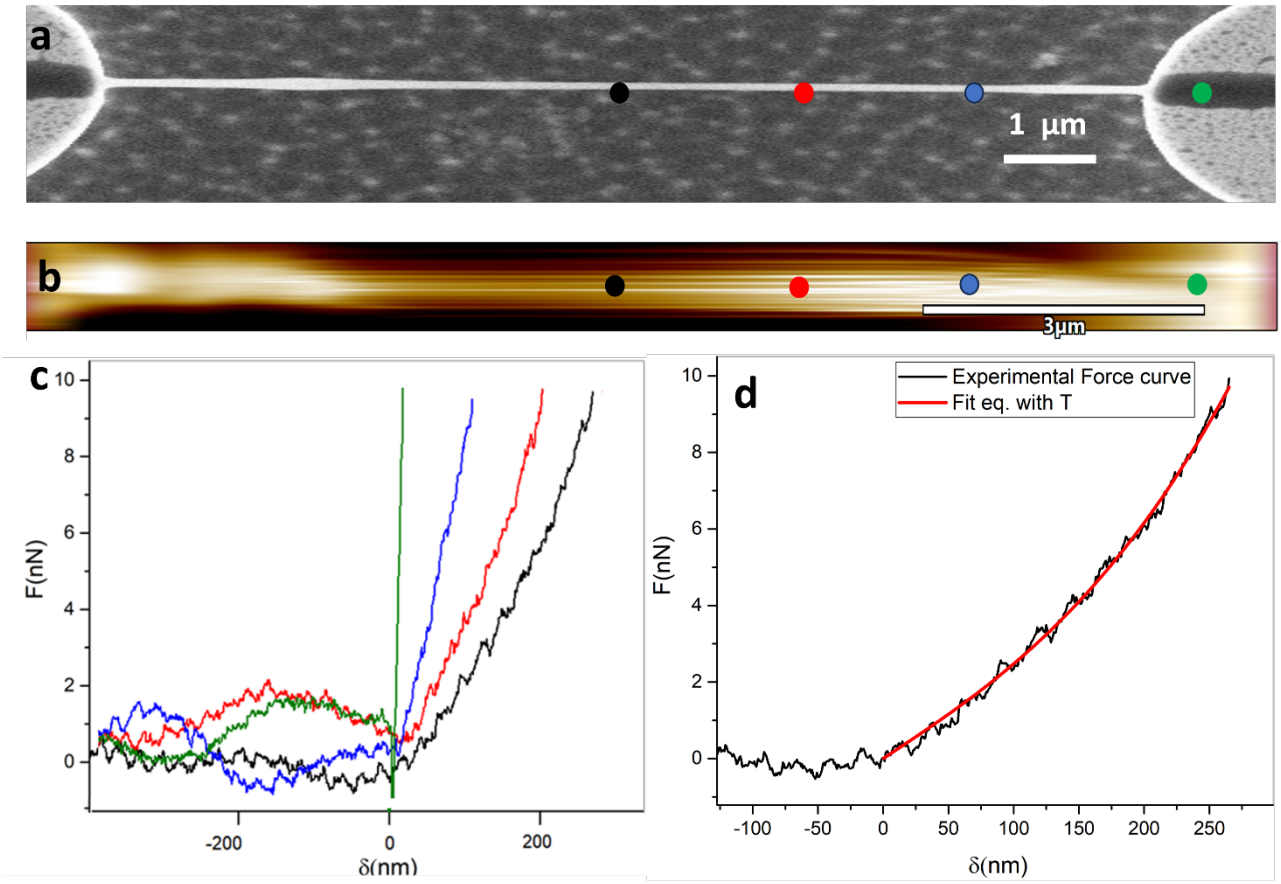

Figure 4. a) SEM and b) AFM imaging in tapping mode of bundle A (diameter 94 nm and length 11.67 µm) from pillar to pillar (color map range: 540 nm). c) Evolution of the force curves for bundle A from the pillar to the midpoint of the beam: the curve color corresponds to the relative position highlighted in a,b). d) Force-curve in the midpoint of the bundle together with the result of the parametric fit with the corrected Heidelberg model.

δ curve in order to obtain the Young's modulus of the structure and the intrinsic T_{in} which then, divided by the bundle cross section, gives the stress σ retained by the structure.

The acquisition of the force curves on the surface of the suspended DNA bundles is challenging since it requires overcoming a series of methodological difficulties. Foremost is the necessity to image a suspended biological nanostructure without breaking it. Key points about how to experimentally succeed in such a delicate measurement are reported in the Supporting Information: from the imaging procedure (Fig. S4) to the F-δ curve extrapolation (Fig. S5), post-processing (Fig. S6) and fit (Fig. S7).

The analysis was performed on 7 bundles composed of DNA molecules at 50% of methylation, suspended in PBS. Fig. 4a shows the SEM image of a bundle with D = 94 nm and L = 11.67 μm (Bundle A in Table 2), while Fig. 4b reports the corresponding AFM image in tapping mode. As described in Fig. S4, the convolution of the lateral part of the tip with the bundle when the tip scans in the void prevents acquisition of a reliable image of the edges of the bundle. However, such imaging was suitable for selecting the four different axial positions where force-deflection F-δ curves were acquired, starting from the pillar up to the midpoint (colored circles in Fig. 4b). As shown in Fig. 4c, the force curve taken on the pillar is roughly vertical (green), as expected for a non-deformable material. In contrast, the deflection of the bundle increases approaching the bundle midpoint, where the highest bending deformation occurs for the same applied force (set to 10nN). In the case of bundle A, the deflection of the beam in the midpoint was δ = 265 nm, i.e. nearly three times the diameter of the beam and thus fully justifying the onset of the non-linear behavior of the curve. Fig. 4d reports the same F-δ curve in the midpoint, together with the parametric fit of the contact portion. To take into account the uncertainty related to the definition of the contact point (always arbitrary to some extent), the same procedure was repeated with three other contact

points and the values of E and T extracted from each fit were averaged (± their standard deviation). More details are given in the Supporting Information (Fig. S7). The average Young's modulus of bundle A was 4.86 ± 0.32 GPa , a value perfectly in line with the one found by Stassi et al.[15] by means of the vibrometric analysis in the case of unstressed DNA bundles. In contrast, the intrinsic tension of the same bundle was 48.94 ± 10.63 nN, almost five times the applied load and corresponding to a tensile stress σ of 7.10 ± 1.5 MPa. Therefore, the AFM force curve analysis confirms the expectation dictated by vibrational analysis, giving a clearly non-negligible value of stress that is in line with extrapolation from eq. (2). As a further evidence for the presence of tensile stress, inserting the diameter and length of bundle A along with the fitted values of E and σ, into eq. (2), gives a theoretical resonance frequency for this nanoresonator of 3.20 ± 0.34 MHz. Such a value perfectly falls in the range of experimental resonance frequencies found for DNA bundles at 50% of methylation reported in Fig. 2c.

Table 2 reports the sizes of the other six analyzed bundles together with the measured displacement d in the midpoint, found for an applied force of 10nN, and the fitted E and σ, spanning respectively from 3 to 12 GPa and from 6 to 11 MPa. The last column of Table 2 reports the calculated resonance frequencies for the DNA nanoresonators under investigation, which roughly goes from 2.8 MHz up to 3.8 MHz. This is again in line with the experimental range of similar methylation (last line in Table 1). It is worth noting that bundles B and C have approximately the same dimensions, but bundle B retained a tensile stress 4 MPa higher than bundle C, thus resulting in a theoretical resonance frequency of almost 1 MHz higher.

To summarize, the AFM analysis shed light on the high variability of the mechanical properties of suspended DNA bundles, since it quantified the Young's modulus and residual tensile stress from F-δ curves. Such results show that a careful control of tensile stress is needed to reduce the

variability of resonance frequency that is currently hampering the application of DNA nanoresonators to epigenetic studies.

Table 2. Geometrical parameters, AFM force-curve results and theoretical resonance frequencies for seven DNA bundles at 50% of methylation.

Bundle	***L* (μm)**	***D* (nm)**	***δ* (nm)**	***E* (GPa)**	***σ* (MPa)**	**Calculated f_1 (MHz)**
A	11.67	94	265	4.86 ± 0.32	7.05 ± 1.53	3.20± 0.34
B	11.90	45	518	5.07 ± 0.12	10.9 ± 1.1	3.85± 0.19
C	12.10	56	556	3.53± 0.11	6.01 ± 0.67	2.82±0.15
D	12.00	56	560	2.99 ± 0.07	7.43 ± 0.76	3.16±0.16
E	11.40	88	235	12.06 ± 0.65	8.45 ± 1.11	3.63±0.23
F	12.00	70	401	4.92± 0.09	7.54 ± 1.09	3.19±0.23
G	12.40	66	334	9.23± 0.33	7.75 ± 1.38	3.14±0.28

Conclusion

The results of this investigation lay the groundwork for distinguishing large changes in DNA methylation levels by means of vibrometric analysis. In fact, it is possible to distinguish three different families of bundles composed of DNA at 50, 25 and 0% methylation according to their average resonance frequencies. The method proposed here would solve issues inherent in the current epigenetic approaches, since the SHS suspension process is able to concentrate the DNA in solution to a well-defined region, up to the attomolar level, thus removing the necessity of amplifying the desired DNA sequence. Furthermore, this method is real time, label free, and designed to analyze long DNA sequences, such as the nucleic acids extracted from patient cells.

Even if the observed high variability of the resonance frequencies prevents further punctual epigenetic studies, where a rigorous target quantification is foreseen, the nature of such variability has been investigated and is now defined. By means of AFM force curve analysis, it was verified that the resonance frequency of each bundle is influenced by the presence of a residual and variable tensile stress retained by the DNA bundle. This tensile stress is a result of the suspension process in which the DNA molecules are pulled between one pillar and the proximal one.

In order to establish the vibrometric analysis of the suspended DNA bundles as an efficient tool for large scale epigenetic studies, it is necessary to compare the resonance frequencies of a large number of exemplars. This requires a method to tune the residual tensile stress in a controlled way. Possible solutions could come from the semiconductor industry, where the residual stress in thin films is typically tuned with *ex post* heating ramps and/or applying a mechanical bending to the whole substrate. Alternatively, the DNA bundles could be pinned to the pillars, thanks to nanodeposition tools (like Focused Ion Beam), and then put in contact again with solution drops that have a different salt concentration and surface tension.

AUTHOR INFORMATION

Corresponding Author

*Carlo Ricciardi: carlo.ricciardi@polito.it

Author Contributions

F.L. and C.R. conceived the experiment. F.L, M.M, B.R. and C.Y.R. managed DNA bundles preparation. F.L. performed all the measurements. Nanomechanical data were analyzed with S.S., E.D.F. and C.R., AFM data with P.D.A. J.E.S. provided the theoretical interpretation of AFM force curves. F.L. wrote the draft and all authors contributed to finalizing the manuscript.

Supporting information: graphical representation of DNA bundles on SHS; additional experimental results: diameter distribution, modal ratios, AFM procedures and data analysis; tables with all the data.

Acknowledgment:

This publication is part of the project NODES which has received funding from the MUR – M4C2 1.5 of PNRR with grant agreement no. ECS00000036. This research has been co-funded by European Union - Next Generation EU Programme within the projects SOE_0000167 and P2022CBHZK (PRIN 2022 PNRR). Work at the Molecular Foundry was supported by the Office of Science, Office of Basic Energy Sciences, of the U.S. Department of Energy under Contract No. DE-AC02-05CH11231.

References

(1) Feinberg, A. P. The Key Role of Epigenetics in Human Disease Prevention and Mitigation. *N. Engl. J. Med.* **2018**, *378* (14), 1323–1334. https://doi.org/10.1056/nejmra1402513.

(2) Moore, L. D.; Le, T.; Fan, G. DNA Methylation and Its Basic Function. *Neuropsychopharmacology* **2013**, *38* (1), 23–38. https://doi.org/10.1038/npp.2012.112.

(3) Lister, R.; Pelizzola, M.; Dowen, R. H.; Hawkins, R. D.; Hon, G.; Tonti-Filippini, J.; Nery, J. R.; Lee, L.; Ye, Z.; Ngo, Q. M.; Edsall, L.; Antosiewicz-Bourget, J.; Stewart, R.; Ruotti, V.; Millar, A. H.; Thomson, J. A.; Ren, B.; Ecker, J. R. Human DNA Methylomes at Base Resolution Show Widespread Epigenomic Differences. *Nature* **2009**, *462* (7271), 315–322. https://doi.org/10.1038/nature08514.

(4) Kobori, T.; Iwamoto, S.; Takeyasu, K.; Ohtani, T. Unmethylated and Methylated CpG Dinucleotides Distinctively Regulate the Physical Properties of DNA. *Biopolymers* **2007**, *85* (4), 392–406. https://doi.org/10.1002/bip.

(5) Tost, J. DNA Methylation: An Introduction to the Biology and the Disease-Associated Changes of a Promising Biomarker. *Mol. Biotechnol.* **2010**, *44* (1), 71–81. https://doi.org/10.1007/s12033-009-9216-2.

(6) Lister, R.; Mukamel, E. A.; Nery, J. R.; Urich, M.; Puddifoot, C. A.; Johnson, N. D.; Lucero, J.; Huang, Y.; Dwork, A. J.; Matthew, D.; Yu, M.; Tonti-filippini, J.; Heyn, H.; Hu, S.; Wu, J. C. Epigenetic Reconfigulation in Mammlian Brain Development. *Science (80-.).* **2013**, *341* (6146), 1–21.

(7) Schmidt, R. J.; Schroeder, D. I.; Crary-Dooley, F. K.; Barkoski, J. M.; Tancredi, D. J.; Walker, C. K.; Ozonoff, S.; Hertz-Picciotto, I.; Lasalle, J. M. Self-Reported Pregnancy Exposures and Placental DNA Methylation in the MARBLES Prospective Autism Sibling Study. *Environ. Epigenetics* **2016**, *2* (4), 1–10. https://doi.org/10.1093/eep/dvw024.

(8) Jones, P. A.; Baylin, S. B. The Fundamental Role of Epigenetic Events in Cancer. *Nat. Rev. Genet.* **2002**, *3* (6), 415–428. https://doi.org/10.1038/nrg816.

(9) Souren, N. Y.; Gerdes, L. A.; Lutsik, P.; Gasparoni, G.; Beltm, E.; Salhab, A.; Kmpfel, T.; Weichenhan, D.; Plass, C.; Hohlfeld, R.; Walter, J. DNA Methylation Signatures of Monozygotic Twins Clinically Discordant for Multiple Sclerosis. *Nat. Commun.* **2019**, *10* (1), 1–12. https://doi.org/10.1038/s41467-019-09984-3.

(10) Paul, D. S.; Teschendorff, A. E.; Dang, M. A. N.; Lowe, R.; Hawa, M. I.; Ecker, S.; Beyan, H.; Cunningham, S.; Fouts, A. R.; Ramelius, A.; Burden, F.; Farrow, S.; Rowlston, S.; Rehnstrom, K.; Frontini, M.; Downes, K.; Busche, S.; Cheung, W. A.; Ge, B.; Simon, M. M.; Bujold, D.; Kwan, T.; Bourque, G.; Datta, A.; Lowy, E.; Clarke, L.; Flicek, P.; Libertini, E.; Heath, S.; Gut, M.; Gut, I. G.; Ouwehand, W. H.; Pastinen, T.; Soranzo, N.; Hofer, S. E.; Karges, B.; Meissner, T.; Boehm, B. O.; Cilio, C.; Larsson, H. E.; Lernmark, .; Steck, A. K.; Rakyan, V. K.; Beck, S.; Leslie, R. D. Increased DNA Methylation Variability in Type 1 Diabetes across Three Immune Effector Cell Types. *Nat. Commun.* **2016**, *7*. https://doi.org/10.1038/ncomms13555.

(11) Ryu, H. W.; Lee, D. H.; Won, H. R.; Kim, K. H.; Seong, Y. J.; Kwon, S. H. Influence of Toxicologically Relevant Metals on Human Epigenetic Regulation. *Toxicol. Res.* **2015**, *31* (1), 1–9. https://doi.org/10.5487/TR.2015.31.1.001.

(12) Beccaria et al.; Bracaglia. DNA Methylation Correlates of PTSD: Recent Findings and Technical Challenges. *Physiol. Behav.* **2017**, *176* (5), 139–148. https://doi.org/10.1016/j.pnpbp.2018.11.011.DNA.

(13) Dias, B. G.; Ressler, K. J. Parental Olfactory Experience Influences Behavior and Neural Structure in Subsequent Generations. *Nat. Neurosci.* **2014**, *17* (1), 89–96. https://doi.org/10.1038/nn.3594.

(14) Šestáková, Š.; Šálek, C.; Remešová, H. DNA Methylation Validation Methods: A Coherent Review with Practical Comparison. *Biol. Proced. Online* **2019**, *21* (1), 1–11. https://doi.org/10.1186/s12575-019-0107-z.

(15) Stassi, S.; Marini, M.; Allione, M.; Lopatin, S.; Marson, D.; Laurini, E.; Pricl, S.; Pirri, C. F.; Ricciardi, C.; Di Fabrizio, E. Nanomechanical DNA Resonators for Sensing and Structural Analysis of DNA-Ligand Complexes. *Nat. Commun.* **2019**, *10* (1), 1–10. https://doi.org/10.1038/s41467-019-09612-0.

(16) Legittimo, F.; Marini, M.; Stassi, S.; Di Fabrizio, E.; Ricciardi, C. Real-Time Monitoring of Temperature-Dependent Structural Transitions in DNA Nanomechanical Resonators: Unveiling the DNA-Ligand Interactions for Biomedical Applications. *ACS Appl. Nano Mater.* **2023**, *6* (3), 2249–2257. https://doi.org/10.1021/acsanm.2c05601.

(17) Allione, M.; Limongi, T.; Marini, M.; Torre, B.; Zhang, P.; Moretti, M.; Perozziello, G.; Candeloro, P.; Napione, L.; Pirri, C. F.; Di Fabrizio, E. Micro/Nanopatterned Superhydrophobic Surfaces Fabrication for Biomolecules and Biomaterials Manipulation and Analysis. *Micromachines* **2021**, *12* (12), 1–31. https://doi.org/10.3390/mi12121501.

(18) De Angelis, F.; Gentile, F.; Mecarini, F.; Das, G.; Moretti, M.; Candeloro, P.; Coluccio, M. L.; Cojoc, G.; Accardo, A.; Liberale, C.; Zaccaria, R. P.; Perozziello, G.; Tirinato, L.; Toma, A.; Cuda, G.; Cingolani, R.; Di Fabrizio, E. Breaking the Diffusion Limit with Super-Hydrophobic Delivery of Molecules to Plasmonic Nanofocusing SERS Structures. *Nat. Photonics* **2011**, *5* (11), 682–687. https://doi.org/10.1038/nphoton.2011.222.

(19) Accardo, A.; Di Fabrizio, E.; Limongi, T.; Marinaro, G.; Riekel, C. Probing Droplets on Superhydrophobic Surfaces by Synchrotron Radiation Scattering Techniques. *J. Synchrotron Radiat.* **2014**, *21* (4), 643–653. https://doi.org/10.1107/S1600577514009849.

(20) Marini, M.; Allione, M.; Torre, B.; Moretti, M.; Limongi, T.; Tirinato, L.; Giugni, A.; Das, G.; di Fabrizio, E. Raman on Suspended DNA: Novel Super-Hydrophobic Approach for Structural Studies. *Microelectron. Eng.* **2017**, *175*, 38–42. https://doi.org/10.1016/j.mee.2016.12.016.

(21) Marini, M.; Falqui, A.; Moretti, M.; Limongi, T.; Allione, M.; Genovese, A.; Lopatin, S.; Tirinato, L.; Das, G.; Torre, B.; Giugni, A.; Gentile, F.; Candeloro, P.; Di Fabrizio, E. The Structure of DNA by Direct Imaging. *Sci. Adv.* **2015**, *1* (7), 241–277. https://doi.org/10.1126/sciadv.1500734.

(22) Marini, M.; Limongi, T.; Falqui, A.; Genovese, A.; Allione, M.; Moretti, M.; Lopatin, S.; Tirinato, L.; Das, G.; Torre, B.; Giugni, A.; Cesca, F.; Benfenati, F.; Di Fabrizio, E. Imaging and Structural Studies of DNA-Protein Complexes and Membrane Ion Channels. *Nanoscale* **2017**, *9* (8), 2768–2777. https://doi.org/10.1039/c6nr07958j.

(23) Gentile, F.; Moretti, M.; Limongi, T.; Falqui, A.; Bertoni, G.; Scarpellini, A.; Santoriello, S.; Maragliano, L.; Proietti Zaccaria, R.; Di Fabrizio, E. Direct Imaging of DNA Fibers: The Visage of Double Helix. *Nano Lett.* **2012**, *12* (12), 6453–6458. https://doi.org/10.1021/nl3039162.

(24) Hausheer, F. H.; Rao, S. N.; Gamcsik, M. P.; Kollman, P. A.; Colvin, O. M.; Saxe, J. D.; Nelkin, B. D.; Mclennan, I. J.; Barnett, G.; Baylin, S. B. Computational Analysis of Structural and Energetic Consequences of DNA Methylation. *Carcinogenesis* **1989**, *10* (6), 1131–1137. https://doi.org/10.1093/carcin/10.6.1131.

(25) Schmid, S.; Villanueva, L. G.; Roukes, M. L. *Fundamentals of Nanomechanical Resonators*; 2016. https://doi.org/10.1007/978-3-319-28691-4.

(26) Salvetat, J. P.; Briggs, G. A. D.; Bonard, J. M.; Bacsa, R. R.; Kulik, A. J.; Stckli, T.; Burnham, N. A.; Forr, L. Elastic and Shear Moduli of Single-Walled Carbon Nanotube Ropes. *Phys. Rev. Lett.* **1999**, *82* (5), 944–947. https://doi.org/10.1103/PhysRevLett.82.944.

(27) Wong, E. W.; Sheehan, P. E.; Lieber, C. M. Nanobeam Mechanics: Elasticity, Strength, and Toughness of Nanorods and Nanotubes. *Science (80-.).* **1997**, *277* (5334), 1971–1975. https://doi.org/10.1126/science.277.5334.1971.

(28) Wang, S.; Shan, Z.; Huang, H. The Mechanical Properties of Nanowires. *Adv. Sci.* **2017**, *4* (4), 1–24. https://doi.org/10.1002/advs.201600332.

(29) Kis, A.; Mihailovic, D.; Remskar, M.; Mrzel, A.; Jesih, A.; Piwonski, I.; Kulik, A. J.; Benot, W.; Forr, L. Shear and Young's Moduli of MoS2 Nanotube Ropes. *Adv. Mater.* **2003**, *15* (9), 733–736. https://doi.org/10.1002/adma.200304549.

(30) Wu, B.; Heidelberg, A.; Boland, J. J. Mechanical Properties of Ultrahigh-Strength Gold Nanowires. *Nat. Mater.* **2005**, *4* (7), 525–529. https://doi.org/10.1038/nmat1403.

(31) Minot, E. D.; Yaish, Y.; Sazonova, V.; Park, J. Y.; Brink, M.; McEuen, P. L. Tuning Carbon Nanotube Band Gaps with Strain. *Phys. Rev. Lett.* **2003**, *90* (15), 4. https://doi.org/10.1103/PhysRevLett.90.156401.

(32) Moretti, M.; La Rocca, R.; Perrone Donnorso, M.; Torre, B.; Canale, C.; Malerba, M.; Das, G.; Sottile, R.; Garofalo, C.; Achour, A.; Krre, K.; Carbone, E.; Di Fabrizio, E. Clustering of Major Histocompatibility Complex-Class i Molecules in Healthy and Cancer Colon Cells Revealed from Their Nanomechanical Properties. *ACS Nano* **2021**, *15* (4), 7500–7512. https://doi.org/10.1021/acsnano.1c00897.

(33) Heidelberg, A.; Ngo, L. T.; Wu, B.; Phillips, M. A.; Sharma, S.; Kamins, T. I.; Sader, J. E.; Boland, J. J. A Generalized Description of the Elastic Properties of Nanowires. *Nano Lett.* **2006**, *6* (6), 1101–1106. https://doi.org/10.1021/nl060028u.

(34) Mills, S.; Sader, J. E.; Boland, J. J. Material Characterisation of Nanowires with Intrinsic Stress. *Nanotechnology* **2017**, *28* (35), 355706. https://doi.org/10.1088/1361-6528/aa7c31.

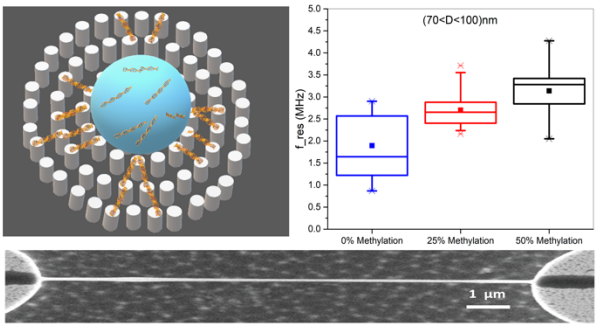

For Table of Contents Only 1